Conductive PVDF/PA6/CNTs Nanocomposites Fabricated by Dual Formation of Cocontinuous and Nanodispersion Structures

Yongjin Li* and Hiroshi Shimizu*

Nanotechnology Research Institute, National Institute of Advanced Industrial Science and Technology (AIST), Tsukuba Central 5, 1-1-1 Higashi, Tsukuba, Ibaraki 305-8565, Japan

Received March 28, 2008; Revised Manuscript Received June 1, 2008

ABSTRACT: A conductive poly(vinylidene fluoride) (PVDF)/polyamide 6 (PA6)/carbon nanotubes (CNTs) composite with a unique hierarchical morphology has been fabricated by the dual formation of cocontinuous and nanodispersion structures using high-shear processing. PVDF and PA6 basically forms cocontinuous structure. The CNTs are exclusively located in the PA6 phase, and numerous PA6 domains with the size ranging from 10 to 150 nm are dispersed in the PVDF phase. The relationships between the physical properties (e.g., electrical conductivity and mechanical properties) and morphology of the composite have been investigated. The results indicate that the formation of PA6 nanodomains in PVDF phase by the high-shear processing not only increases the electrical conductivity but also improves the ductility of the obtained blend nanocomposites.

1. Introduction

Conductive polymer composites consisting of an insulating polymer matrix and an electrically conductive filler have attracted much attention recently. The investigations of conductive polymer composites have mainly focused on decreasing the percolation threshold to lower the cost, improve processability, and enhance the mechanical properties of composites.[1–5] An important way of reducing the percolation threshold of composites is to induce inhomogeneities in the materials.[6–14] For instance, it was reported that carbon black particles could be rejected from crystal regions in semicrystalline polymers, which accordingly decreases the lowest concentration (percolation threshold) of carbon black at which a continuous conducting network was formed.[6,7] A more effective method is the so-called double percolation techniques, in which a two-phase (immiscible) polymer blend was used as the polymer matrix in composites.[8–14] In this type of polymer blend composite, either one of the two polymer phases is continuous and a conducting filler is selectively localized in the continuous phase or the two phases are cocontinuous and the filler has preferably to be in one phase[8–12] or at the interface.[13,14] However, this type of conductive polymer composite usually exhibits poor mechanical properties due to incompatibilities between component polymers.[10,12] Moreover, the formed morphologies are sometimes not stable upon thermal annealing at melting temperature. Therefore, the fabrication of a thermally stable cocontinuous conductive polymer composite with further reduced filler loading content and improved mechanical properties still poses significant scientific and industrial challenges.

We have very recently developed a high-shear processing technique for polymer compounding. In our previous studies, we reported that high-shear processing could improve the compatibility of an immiscible polymer blend and form a nanostructured polymer blend material with greatly improved physical properties.[15] In addition, it was also found that the high-shear processing is very effective in fabricating highly dispersed polymer nanocomposites without using any additive or surfactant.[16] Carbon nanotubes (CNTs) have been expected as attractive fillers for increasing the electrical conductivity of polymers at relatively low CNT content.[17–20] However, the homogeneous dispersion of CNTs is the most important issue in the preparation of polymer/CNTs composites because pristine CNTs are not soluble in polymers, and they usually tend to aggregate together. In this work, we reported the fabrication of a poly(vinylidene fluoride) (PVDF)/polyamide 6 (PA6)/pristine multiwalled CNTs composites by the dual formation of cocontinuous and nanodispersion structures using the high-shear processing technique. The prepared composites show very unique double percolation structures with markedly reduced percolation threshold and significantly improved electrical and mechanical properties. The PVDF/PA6 blend was chosen as the polymer matrix because both PVDF and PA6 are chemically inert in a fuel cell environment.[21,22] Therefore, the fabricated PVDF/PA6/CNTs conductive composites with high electrical conductivity and excellent mechanical properties may be used as bipolar plates in fuel cell systems.

2. Experimental Section

Materials and Sample Preparation. The poly(vinylidene fluoride) (PVDF) and polyamide 6 (PA6) used were commercially available KF850 (Kureha Chemical Co. Ltd., Japan) and A 1030 BRL (Unitika Co. Ltd., Japan), respectively. The purity of the multiwalled carbon nanotubes used is about 95%. The tube diameters are in the range of 10−40 nm with lengths of 5−20 μm. The PVDF/PA6 composition ratio in the blend composites was fixed at 50/50 (w/w). The PVDF/PA6/CNTs blend composites with various CNT contents were prepared via melt compounding using a high-shear extruder, HSE3000mini (Imoto Co., Japan). The loading contents of CNT in this work are based on the entire blend. A feedback-type screw was used in this extruder. The *L*/*D* ratio of the screw was about 1.78. The rotation speed of the screw used in this study was set at 100 and 1000 rpm, which correspond to average shear rates of 147 and 1470 s^{-1}, respectively. The melt compounding was carried out at 240 °C for 2 min using the extruder. The compounded samples were then extruded from a T-die. For physical property measurements, all the extruded samples were hot-pressed at 240 °C to a sheet with the thickness of 500 μm, followed by quenching in ice water. PA6/CNTs composites were also prepared using the same extruder with the screw rotation speed of 1000 rpm at 240 °C.

TEM Characterization. The sections of the PVDF/PA6/CNTs composites were observed and analyzed in a high acceleration voltage transmission electron microscope (TEM), TECNAI G2-F20 (FEI Co.), equipped with an energy-dispersive X-ray (EDX) microanalysis system at 200 kV. For TEM-EDX analysis, electron beams were irradiated onto a small spot (diameter 10 nm), and the emitted X-rays were analyzed with specific EDX spectra counts

* To whom correspondence should be addressed. E-mail: yongjin-li@aist.go.jp; shimizu-hiro@aist.go.jp.

10.1021/ma8006834 CCC: $40.75
Published on Web 06/24/2008

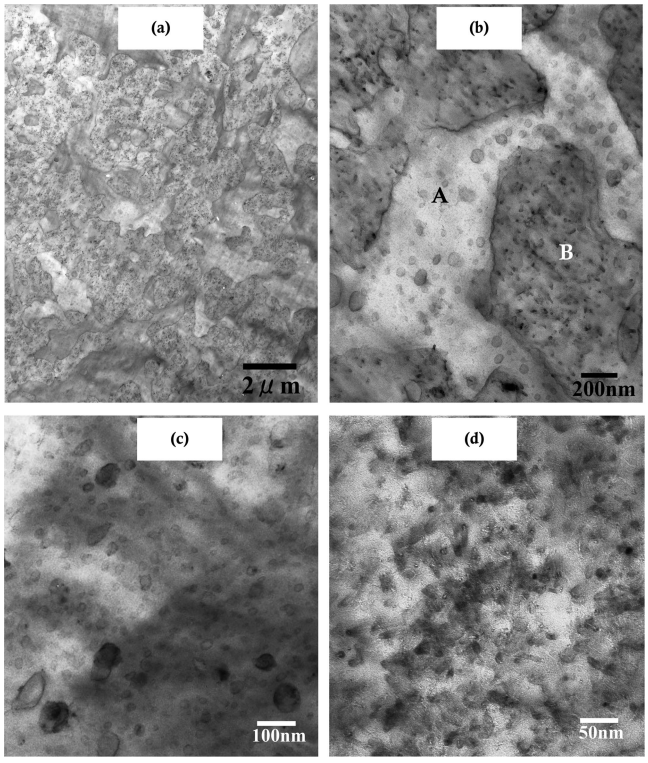

Figure 1. TEM image of high-shear-processed PVDF/PA6/CNTs composites (CNT loading content is 1.8 wt %): (a) at 5000× magnification, (b) at 50 000× magnification, (c) enlarged part of region A in (b), and (d) enlarged part of region B in (b).

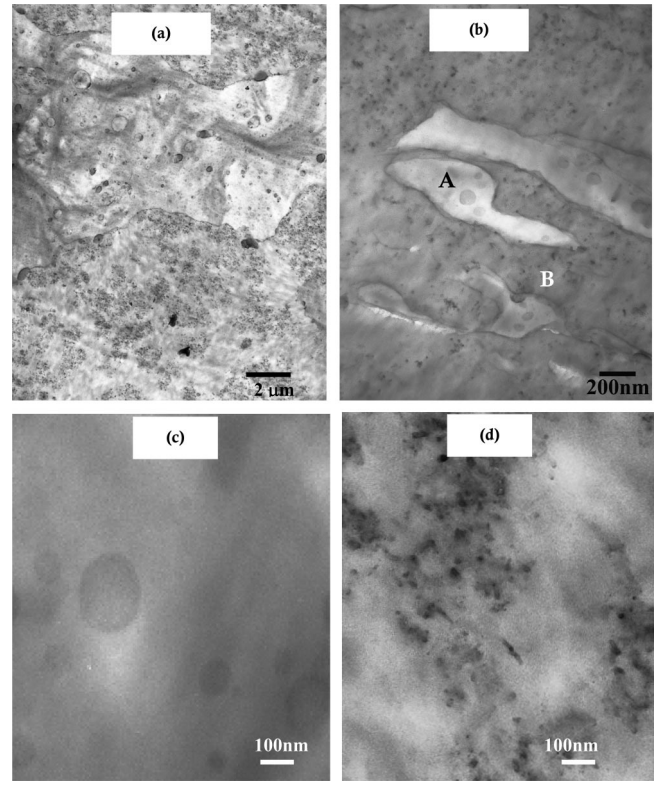

Figure 2. TEM image of the low-shear-processed PVDF/PA6/CNTs composites (CNT loading content is 1.8 wt %): (a) at 5000× magnification, (b) at 50 000× magnification, (c) enlarged part of region A in (b), and (d) enlarged part of region B in (b).

for 10 s. For TEM observation, the sample was stained by two steps to enhance the contrast. First, the trimmed specimen embedded in epoxy resin was stained with solid OsO_4 for 2 h in a sealed glass tube. Next, the corresponding specimen was stained with solid RuO_4 for 15 min. Then, the stained specimen for TEM was cut into about 120 nm sections with an ultramicrotome Reichert ULTRACUT-UCT and a Diatome diamond knife.

Electrical Conductivity Measurement. Two types of characterization apparatus were used in evaluating the electrical conductivity of the prepared composites dependent upon the conductivity of the samples. For the samples with high resistivity, an ADVANTEST R8340A ultrahigh-resistance meter was used. Different voltages were applied on different samples depending on the level of resistivity of the specimens. For the samples with high conductivity, the resistivity of the samples was measured according to the method JIS K7194 (testing method for resistivity of conductive plastics with four-point probe array).

Mechanical Property Measurement. The stress−strain curves were measured using a tensile testing machine, Tensilon UMT-300 (Orientec Co. Ltd., Japan). Dumbbell-shaped specimens were punched from the hot pressed sample for the tensile test. Tensile tests were carried out at a rate of 10 mm/min at 20 °C and 50% relative humidity.

Rheology Measurements. The viscosity measurements of neat PVDF, PA6, and PA6/CNTs were carried out on Advanced Rheometric Expansion System (ARES) in oscillatory shear at 10% strain in the parallel-plate arrangement. The frequency sweeps from 0.1 to 300 rad/s were performed at 240 °C.

Thermal Behavior. Dynamic mechanical properties (DMA) were measured with Rheovibron DDV-25FP-S (Orientec Co. Ltd.) in a stretching mode. The samples were dried at 80 °C for 96 h in the vacuum oven before the measurements. Dynamic storage and loss moduli were obtained at a frequency of 1 Hz and a heating rate of 3 °C/min in the temperature range of −150 to 240 °C. Differential scanning calorimetry (DSC) was carried out under nitrogen flow at a heating or cooling rate of 10 K/min with a Perkin-Elmer DSC-7 differential scanning calorimeter calibrated using the melting temperatures of indium and zinc. The percent crystallinities of both PVDF and PA6 were calculated as the ratio of the heat of fusion (ΔH_f) of the two components to the heat of fusion of the purely crystalline forms of PVDF and PA6 ($\Delta H_f°$). The $\Delta H_f°$ values were taken as 105 J/g for PVDF[23] and 190.9 J/g for PA6.[24]

3. Results and Discussion

Morphological Analysis. Results of our morphological investigation indicate that high-shear-processed PVDF/PA6/CNTs composites have unique hierarchical structures. Figure 1 shows the typical TEM images obtained by changing the magnifications of the PVDF/PA6/CNTs composites processed at a screw rotation speed of 1000 rpm (designated high-shear-processed sample hereafter). As shown in parts a and b of Figure 1, two distinct regions are noted, designated regions A and B, respectively. It is seen that both regions form continuous phase, indicating the basically cocontinuous structures of the prepared blend composites. The phase size of the cocontinuous structures is on the micrometer scale. It is reasonable to conclude that the polymer matrix in region A (white region) is mainly the PVDF phase and that the polymer matrix in region B (dark region) is mainly the PA6 phase because PA6 is more readily stained than PVDF. As shown in Figures 1c,d, the high-magnification TEM images show that CNTs are preferentially located in the PA6 phase and that no CNTs are observed in the PVDF phase, which can be attributed to the higher affinity of CNTs with PA6 than with PVDF. Moreover, few CNTs aggregates are observed, and almost all CNTs are highly dispersed in the PA6 phase. On the other hand, as shown in Figure 1c and in region A of Figure 1b, numerous black domains with sizes from 20 to 150 nm are precisely dispersed in the PVDF phase. The nanodomains were confirmed to be PA6 domains by TEM-EDX analysis (see Figure 3). Therefore, a novel polymer blend composite has been fabricated by the dual formation of cocontinuous and nanodis-

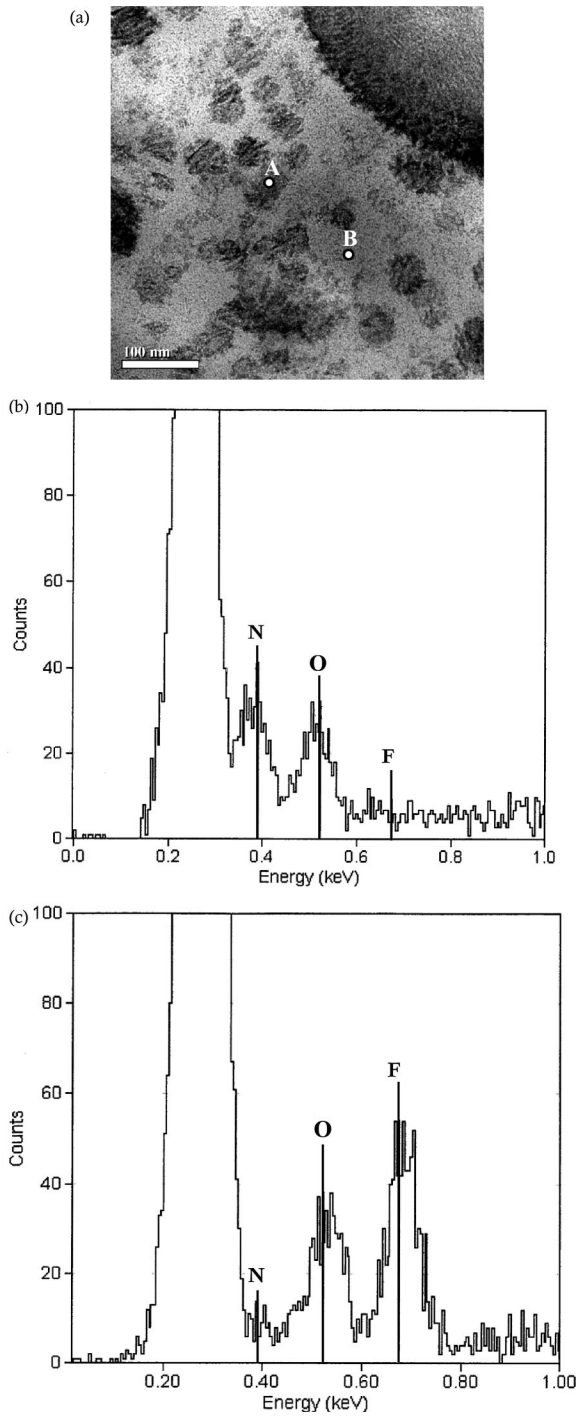

Figure 3. TEM-EDX spectra of the high-shear-processed blend composites: (b) the spectrum corresponds to the A region in (a), and (c) the spectrum corresponds to the B region in (a).

persion structures using high-shear processing. In this composite, PVDF and PA6 basically form the cocontinuous structure on the micrometer scale. The nanoscale structures are further observed in the two phases. CNTs have homogenously and selectively located in the PA6 phase and many PA6 nanodomains with sizes of several tens of nanometers dispersed in the PVDF phase. We found that this hierarchical structure is very stable against thermal annealing. The composite structure processed at a high shear showed no change under the remelt conditions. We will show the effects of the formation of this type of hierarchical morphology on the electrical conductivity and physical properties of the composites in the next section.

For comparison, we also conducted a morphological analysis of a PVDF/PA6/CNTs composite sample processed at a screw rotation speed of 100 rpm (designated low-shear-processed sample), as shown in Figure 2. Note that this screw rotation speed is almost the same as that exerted by most polymer processing techniques used nowadays. The PVDF/PA6 composition ratio and CNT loading content of this low-shear-processed sample are the same as those of the high-shear-processed sample. As shown in Figure 2a, the low-shear-processed sample shows a cocontinuous structure with all CNTs located in the PA6 phase, similar to the high-shear-processed sample. However, two significant differences can be observed with the detailed observation in both PVDF and PA6 phases. First, as shown in Figure 2c, few PA6 nanodomains can be found in the PVDF phase for the low-shear-processed sample. Second, as shown in Figure 2d, the dispersion of the CNTs in the PA6 phase is not very homogeneous, and clear CNTs aggregates can be observed.

To differentiate the component of the nanoparticles in PVDF phase and elucidate the component interactions for the high-shear-processed blend composites, the EDX microanalysis was used for elemental analysis for different parts of the high-shear processed composite, as shown in Figure 3. Figures 3b,c show the EDX spectra of the respective parts designated in Figure 3a. In these figures, the horizontal axis represents the energy corresponding to the specific X-ray emitted and the vertical axis represents intensity counts of the X-ray. The most intense peak observed at 0.28 keV was assigned to the specific X-ray of carbon (C). Figure 3b gives relatively intense peaks at 0.39 and 0.52 keV, originated from nitrogen (N) and oxygen (O), respectively. The fact that both N and O are observed means that the nanodomains are PA6. On the other hand, for the part of the PVDF matrix, very strong fluorine (F) peak at 0.67 keV was found in Figure 3c. Note that N peak can also be observed, indicating some PA6 molecules chains may be inserted in the PVDF matrix. Therefore, the compatibility between PVDF and PA6 is improved by the extremely high mechanical shear stress during processing. One should note that the strong intensity of O peak in Figure 3c might be partially originated from the staining agents (OsO_4 and RuO_4) used for TEM staining.

The morphological differences between the high-shear- and low-shear-processed polymer composites are clearly due to screw rotation speeds used. Numerous investigations have shown that the dispersion of fillers in a polymer matrix is dependent upon the shear stresses exerted on the fillers during melt mixing.[16,25,26] The shear stress can overwhelm the electrostatic and van der Waals interactions in the fillers and lead to the breakup of the filler agglomerates. Therefore, the dispersion of CNTs in PA6 phase for the high-shear-processed sample is more homogeneous than that for the low-shear-processed sample. On the other hand, PA6 can be dispersed in PVDF matrix with the domain size of less than 100 nm by applied high shear stress for the PVDF/PA6 blend without CNT (see Figure S1). Therefore, for the PVDF/PA6/CNTs blend composites, we have successfully combined the two types of structure in one system, and the unique hierarchical morphology was obtained.

It should be mentioned that PVDF/PA6/CNTs composites with CNTs loading less than 0.6 wt % under both the high- and low-shear processing show the typical sea−island morphology where PA6/CNT is the matrix and PVDF forms the domains. The morphological transformation may be attributed to the selectively located CNTs effects on the melt behaviors of the blend system. The cocontinuous structure of a binary polymer blend usually forms within a composition region near the phase inversion, and the composition range is basically governed by the relative melt viscosities of the two components.[27–29] Figure 4 shows the viscosity data for neat PVDF, neat PA6, and PA6 with 1.2 and 3.6 wt % CNTs. It is seen that

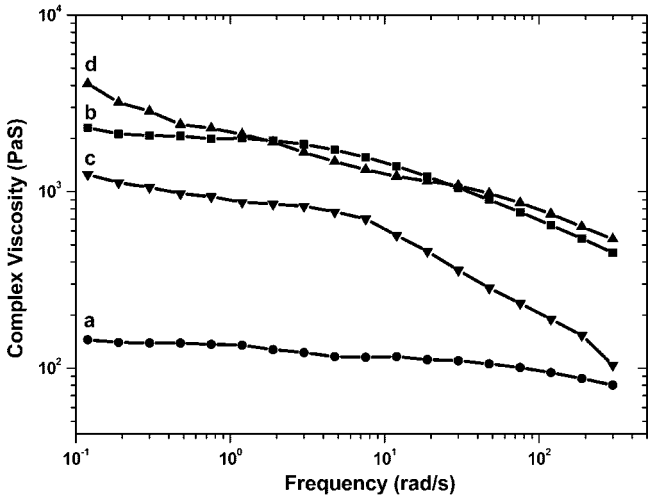

Figure 4. Shear rate dependence of melt viscosity of (a) neat PA6, (b) neat PVDF, (c) PA6/CNTs with 1.2 wt % CNTs, and (d) PA6/CNTs with 3.6 wt % CNTs.

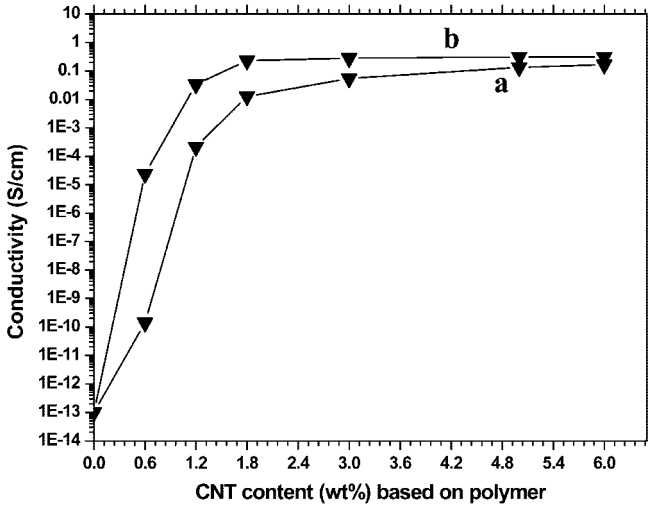

Figure 5. Electrical conductivity of (a) low-shear-processed PVDF/PA6/CNTs composites and (b) high-shear-processed PVDF/PA6/CNTs composites.

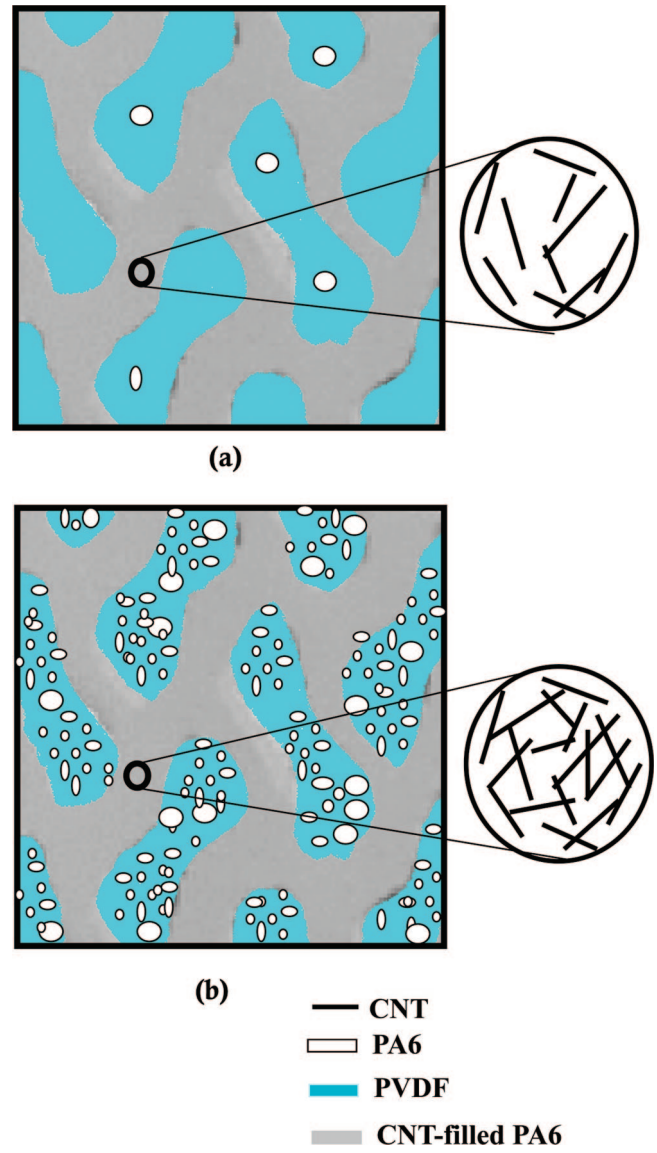

Figure 6. Morphological schematic representations of PVDF/PA6/CNTs composites processed under (a) low shear and (b) high shear.

PVDF is much more viscous than PA6; thus, PVDF tends to form domains for PVDF/PA6 (50/50 w/w) blends without CNTs. The addition of CNTs in PA6 significantly increases the melt viscosity of PA6 phase, and a phase transformation from sea−island to cocontinuous occurs upon adding more than 1.2 wt % CNTs into the blends.

Electrical Conductivity. The novel nanostructured cocontinuous PVDF/PA6/CNTs composites exhibit drastically increased electrical conductivity. Figure 5 shows the volume conductivities for PVDF/PA6/CNTs composites processed under low shear and high shear as functions of the CNTs loading content. As expected, the electrical conductivities of all the composites strongly depend on the CNT loading content. For the high-shear-processed samples, conductivity markedly increases upon the addition of a small amount of CNTs to the composites. Conductivity increases from 1×10^{-13} S/cm for the PVDF/PA6 blend without CNT to 0.4 S/cm for the same blend with a loading content of about 1.8 wt % CNTs. Upon further increasing CNT loading content, conductivity levels off at an almost constant value, indicating the formation of CNT networks for electron transport. It can be calculated that the percolation threshold is attained at a CNT loading content of about 0.8 wt %, which, in view of the multiwall CNTs, is pretty low compared with that reported in some recent studies.[11,12,17,18] For the low-shear-processed sample, conductivity shows similar changes with the CNT loadings content. However, the conductivities are much lower than those for the high-shear-processed sample at the same CNT loading content. At a 0.6 wt % CNT loading, the conductivity of the high-shear-processed sample is about 5 decades higher than that of the low-shear-processed sample. Moreover, the percolation threshold of the low-shear-processed sample is about 1.7 wt %, which is almost 2 times that of the high-shear-processed sample.

It is clear that the morphological difference between the two samples accounts for the significant variation in electrical conductivity. On the one hand, carbon nanotubes are well exfoliated and highly dispersed in the PA6 phase in the high-shear-processed sample, in comparison with those in the low-shear-processed sample. Therefore, an interconnecting CNT conducting network is readily formed at lower CNT concentrations for the high-shear-processed sample. On the other hand, numerous PA6 nanodomains are observed in the PVDF phase for the high-shear-processed sample, which means that some parts of PA6 moved in the PVDF phase as induced by the high-shear stress during the melt mixing. Although CNTs have a higher affinity with PA6 than with PVDF, they still cannot locate

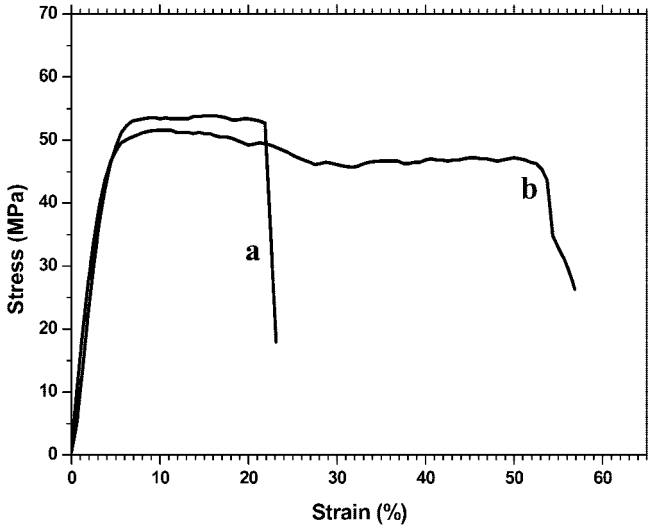

Figure 7. Stress−strain curves of (a) low-shear-processed PVDF/PA6/CNTs composites and (b) high-shear-processed PVDF/PA6/CNTs composites.

in PA6 nanodomains with sizes less than 200 nm in the PVDF phase because the lengths of a single carbon nanotube range from 5 to 20 μm, which is much longer than the diameter of PA6 nanodomains. Therefore, the actual CNT concentration in the PA6 matrix in the high-shear-processed sample is higher than that in the low-shear-processed sample. The morphological schematic representation of the PVDF/PA6/CNTs composites processed under different shear rates is shown in Figure 6. As one can see from the figure, the CNT concentration in PA6 phase in the high-shear-processed sample is higher than that in the low-shear-processed sample owing to the formation of nanodomains in the PVDF phase.

Mechanical Properties. Generally, polymer blend composites with selectively located fillers show poor mechanical properties and low ductility because of the weak interface between the two phases.[10,12] Figure 7 exhibits a comparison of the stress−strain curves for the high-shear- and low-shear-processed PVDF/PA6/CNTs composites. At least five samples were used for each measurement. Only reproducible results are given in Figure 7 for the comparison. No clear yielding behavior for the both composites was observed. The blend composites fabricated using different screw rotation speeds have almost the same modulus, but different elongations at break. The elongation at break for the high-shear-processed composites is about 200% higher than that for the low-shear-processed composites. The marked improvement in the physical properties of the composites is believed to be related to the improved compatibility between PVDF and PA6 induced by the high-shear processing.

Thermal Behavior. Figure 8 shows the temperature dependence of dynamic loss in dynamic mechanical analysis, tan δ, of the blend nanocomposites prepared under high- and low-shear-processed samples. The glass transition temperature (T_g) of PA6 for the low-shear processed composition is 64.6 °C, almost same as that for neat PA6, indicating the immiscibility between PA6 and PVDF for the low-shear-processed sample. In contrast, the high-shear-processed blend composite gives the T_g of 54 °C, which is significantly lower than neat PA6. This demonstrates that molecular chains of PA6 might be partially dissolved in the PVDF phase by the high-shear stress during melt compounding, which has confirmed by TEM-EDX analysis in Figure 3. The dynamic loss modulus peak at −41 °C peak is originated from the glass transition of PVDF. The T_g of PVDF is also a little increased with increasing the shear rate, but the shift is smaller for the glass transition of PVDF than for that of PA6.

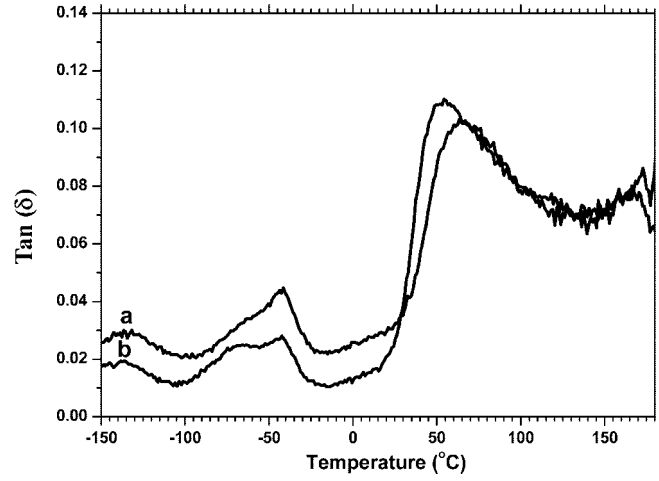

Figure 8. Temperature dependence of dynamic loss of low-shear- (a) and high-shear-processed (b) PVDF/PA6/CNTs composites.

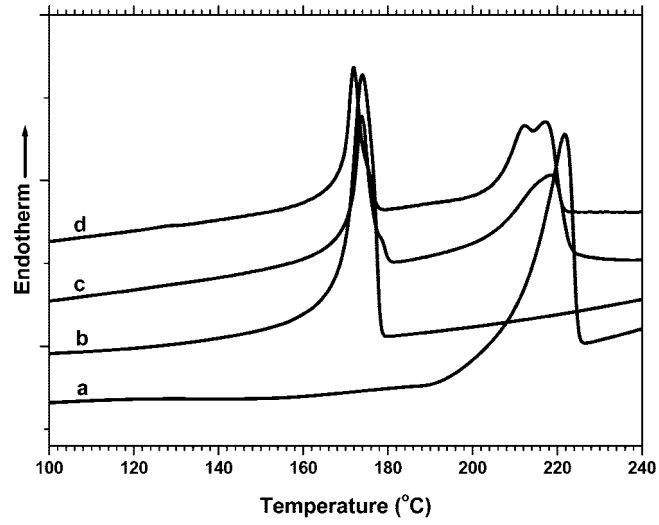

Figure 9. DSC curves of melt-quenched samples of (a) PA6, (b) PVDF, (c) low-shear-processed blend composite with 1.8 wt % CNTs, and (d) high-shear-processed blend composite with 1.8 wt % CNTs.

Table 1. Melting Temperature and Crystallinity of PVDF and PA6 in the Blend Nanocomposites

	neat PVDF	neat PA6	low-shear-processed nanocomposites[a]	high-shear-processed nanocomposites[a]
T_{mPVDF} (°C)	174.4		173.9	171.6
T_{mPA6} (°C)		222	219.2	216.8
χ_{cPVDF} (%)	45.7		43.1	39.2
χ_{cPA6} (%)		35.2	31.8	24.6

[a] The CNT loading is 1.8 wt %.

Figure 9 compares DSC curves of the blend composites prepared under high- and low-shear-processed samples as well as neat PVDF and neat PA6. Table 1 demonstrates the melting peaks and the crystallinities of PVDF and PA6 in the blend nanocomposites as well as those in neat samples. High-shear-processed sample shows clearly decreased melting temperatures for both PVDF and PA6 as compared with the low-shear-processed sample. Moreover, PA6 crystallinity in the high-shear-processed nanocomposites was much lower than in neat PA. These results again indicate the improved compatibility between PA6 and PVDF by the high-shear processing.

4. Conclusion

In summary, we have found that high-shear processing can lead to the formation of novel nanostructured cocontinuous conductive polymer composites, PVDF/PA6/CNTs composites, in which conductive CNTs are homogeneously and selectively located in the PA6 phase and numerous PA6 nanodomains are dispersed in the PVDF phase. The nanostructured conductive polymer composites have a unique combination of properties such as electrical conductivity, ductility, and stiffness (modulus), which are impossible to achieve with classical processing techniques.

Supporting Information Available: TEM image for high-shear-processed PVDF/PA6 blend with no CNT loading. This material is available free of charge via the Internet at http://pubs.acs.org.

References and Notes

(1) Ponomarenko, A. T.; Shevchenko, V. G.; Enikolopyan, N. S. *Adv. Polym. Sci.* **1990**, *96*, 25.
(2) Klupper, M. *Adv. Polym. Sci.* **2003**, *164*, 1.
(3) Li, D.; Wang, Y. L.; Xia, Y. N. *Adv. Mater.* **2004**, *16*, 361.
(4) Konishi, Y.; Cakmak, A. *Polymer* **2006**, *47*, 5371.
(5) Xi, Y.; Bin, Y. Z.; Chiang, C. K.; Matsuo, M. *Carbon* **2007**, *45*, 1302.
(6) Luo, Y. L.; Wang, G. C.; Zhang, B. Y.; Zhang, Z. P. *Eur. Polym. J.* **1998**, *34*, 1221.
(7) Wignall, G. D. *J. Mater. Sci.* **1990**, *25*, 69.
(8) Sumita, M.; Sakata, K.; Asai, S.; Miyasaka, K.; Nakagawa, H. *Polym. Bull.* **1991**, *25*, 265.
(9) Levon, K.; Margolina, A.; Patashinsky, A. Z. *Macromolecules* **1993**, *26*, 4061.
(10) Meincke, O.; Kaempfer, D.; Weickmann, H.; Friedrich, C.; Vathauer, M.; Waith, H. *Polymer* **2004**, *45*, 739.
(11) Potschke, P.; Bhattacharyya, A. R.; Janke, A. *Carbon* **2004**, *42*, 965.
(12) Wu, M.; Shaw, L. L. *J. Power Sources* **2004**, *136*, 37.
(13) Gubbels, F.; Blacher, S.; Vanlathem, E.; Jerome, R.; Deltour, R.; Brouers, F.; Teyssie, Ph. *Macromolecules* **1995**, *28*, 1559.
(14) Gubbels, F.; Jerome, R.; Teyssie, Ph.; Vanlathem, E.; Deltour, R.; Calderone, A.; Parente, V.; Bredas, J. L. *Macromolecules* **1994**, *27*, 1972.
(15) (a) Shimizu, H.; Li, Y. J.; Kaito, A.; Sano, H. *Macromolecules* **2005**, *38*, 7880. (b) Shimizu, H.; Li, Y. J.; Kaito, A.; Sano, H. *J. Nanosci. Nanotechnol.* **2006**, *6*, 3923. (c) Li, Y. J.; Shimizu, H. *Eur. Polym. J.* **2006**, *42*, 3202. (d) Li, Y. J.; Shimizu, H.; Furumichi, T.; Takahashi, Y.; Furukawa, T. *J. Polym. Sci., Part B: Polym. Phys.* **2007**, *45*, 2707.
(16) (a) Li, Y. J.; Shimizu, H. *Polymer* **2007**, *48*, 2203. (b) Chen, G. X.; Li, Y. J.; Shimizu, H. *Carbon* **2007**, *45*, 2334.
(17) (a) Potschke, P.; Bhattacharyya, A. R.; Janke, A. *Polymer* **2003**, *44*, 8061. (b) Potschke, P.; Pegel, S.; Claes, M.; Bonduel, D. *Macromol. Rapid Commun.* **2008**, *29*, 244.
(18) Sandler, J.; Shaffer, M. S. P.; Prasse, T.; Bauhofer, W.; Schulte, K.; Windle, A. H. *Polymer* **1999**, *40*, 5967.
(19) Ajayan, P. M.; Schadler, L. S.; Giannaris, C.; Rubio, A. *Adv. Mater.* **2000**, *12*, 750.
(20) Moniruzzaman, M.; Winey, K. I. *Macromolecules* **2006**, *39*, 5194.
(21) Cunningham, B. D.; Baird, D. G. *J. Power Sources* **2007**, *168*, 418.
(22) Kuo, J. K.; Chen, C. K. *J. Power Sources* **2006**, *162*, 207.
(23) Nakagawa, K.; Ishida, Y. *J. Polym. Sci., Polym. Phys.* **1973**, *11*, 2153.
(24) Inoue, M. *J. Polym. Sci., Polym. Chem.* **1963**, *1*, 2697.
(25) Chawla, K. K. *Composite Materials Science and Engineering*; Spinger-Verlag: New York, 1987.
(26) Cho, J. W.; Paul, D. R. *Polymer* **2001**, *42*, 1083.
(27) Paul, D. R.; Barlow, J. W. *J. Macromol. Sci., Rev. Macromol. Chem.* **1980**, *C18*, 109.
(28) Utracki, L. A. *J. Rheol.* **1991**, *35*, 1615.
(29) Tomotiki, S. *Proc. R. Soc. London, Ser. A* **1935**, *150*, 322.

MA8006834